# Fuzzy Improvement on Luenberger Observer Based Induction Motor Parameters Estimation for High Performances Sensorless Drive

**Zakaria Boulghasoul[1] · Zineb Kandoussi[2] · Abdelhadi Elbacha[1] · Abdelouahed Tajer[1]**

## Abstract

In this paper we present a new improved sensorless vector control of induction motor based on an improved adaptive Luenberger observer. The proposed observer is designed to estimate both speed and motor parameters from measured stator currents, stator voltages and estimated rotor fluxes. The proposed sensorless drive has for purpose to compensate at the same time both stator resistance and rotor time constant inverse variation, which change during operation. Indeed, in the proposed adaptive Luenberger observer, a Fuzzy Logic Controller will be adopted as an adaptation mechanism. The proposed observer stability is proved by the Lyapunov's theorem and its feasibility is verified by series of experimental tests. The relevant results and the effectiveness of the improved system are clearly shown through obtained experimental results with an induction motor of 1 kW driven by dSPACE system.

**Keywords** Induction motor · Sensorless vector control · Luenberger observer · Fuzzy logic control · Lyapunov criterion · Parameters identification

## 1 Introduction

Due to the high cost of permanent magnet, induction motors (IMs) have attracted attention of modern industrial process designers. They have found their place in a wide range of industrial applications such as electric vehicles, transportation and aerospace industries. Induction motors offer several advantages compared to other motors such us ease of manufacturing, reliability, ruggedness, less maintenance and the most important its low price. However, IMs are highly coupled and multivariable systems. Consequently, parallel control of various variables is required to efficiently control the rotor speed and the torque. The reason why, it is essential to artificially obtain a decoupling between the flux and the torque using Field Oriented Control (FOC) for fast dynamic response and for better performances [29].

The use of a speed sensor in induction motor for precise signal measurement is required for closed loop speed drive. Therefore the presence of a speed sensor (encoder) can be an inconvenient. Instead of its extra cost, it leads to increase sensitivity to vibration and limits the application of induction motor in a relatively harsh environment. Thus, especially in the two last decades, and due to the recent advances in DSP, FPGA and ASICs technologies, sensorless control is becoming attractive to find solutions allowing to induction motor to operate at high performance without measurement of mechanical variables [26, 28].

In order to overcome these challenges, recently, various techniques for speed estimation that varies from open-loop to closed-loop estimator have been proposed and applied in medium and high speed regions. Among these techniques, Model Reference Adaptive System Observer (MRAS) [2, 32, 35, 36, 38] which is one of the popular observer due to its simplicity and ease of implementation in many forms (MRAS based rotor flux, Back EMF, reactive power…). However, at low speed region, inverter nonlinearity and uncertainties caused by parameters variation, especially the stator resistance, make the MRAS observer not able to provide required performances.

The Sliding Mode observer [8, 15, 25, 27] is one of the speed observer that gained a great attention in the last

✉ Zakaria Boulghasoul
   z.boulghasoul@gmail.com

[1] System Engineering and Applications Laboratory (SEAL), National School of Applied Sciences, Cadi Ayyad University, B.P 575, Av. Abdelkarim khattabi, 40000 Marrakech, Morocco

[2] Private University of Marrakech, Km 13, route d'Amizmiz, 42312 Marrakech, Morocco

years because of its insensitivity against motor parameters variation and its robustness. However, this observer suffers from chattering phenomenon and requires an infinite switching rate. The Extended Kalman Filter [3, 11] and/or the Unscented Kalman Filter [33] as a speed observer, show high improvements in estimation for all region. But their main drawback is the use of a non-constant gain updated over time that increases computational complexity.

The high gain observer [12] which is also used for induction motor variables estimation, provides the advantage of using only one parameter for dynamic system adjustment. However, to find the optimal value of this parameter there is no clear analytical study that has been reported, only trial and error method that can be used for this issue.

Artificial neural networks have been also used for performance improvement of the induction motor parameters estimation [6, 7, 23]. Nevertheless, depending on the range of the operational speed and on the application, the number of neurons in hidden layer can be increased and then the computational complexity.

All these approaches differ with respect to accuracy, robustness, and sensitivity against model parameters variation especially stator and rotor resistances. Thus, the online identification of these parameters have attracted the research community in the field of robust sensorless drive. To overcome problems with machine model based techniques, methods with high-signal frequency injection were born [14, 24]. The advantages of these techniques are related to their insensitivity to parameters variation and their high precision at very low speed region. However, they require a special system for a real time implementation.

Out of various approaches, the Luenberger observer (LO) that was originally published by David G. Luenberger [21], received a lot of attention from other researchers [2, 9, 17–19, 22, 30]. Among the developed LO structures, we find the adaptive Luenberger observer which is one of the most popular adaptive observers used in sensorless motor control applications. It presents high performances and good stability, without forgetting its ease of implementation and low computational effort. Its structure is based on the IM model that estimates the state variables on the basis of different sets of input variables and an adaptive mechanism (AM).

In practice, considerable variations of stator resistance and rotor resistance/rotor time constant (RTC) take place when the motor temperature changes at varying load or speed or air temperature surrounding the motor, that's why online adaptation of these quantities has improved the performance of the induction motor sensorless drive.

In literature, the majority of the proposed schemes, whether for speed estimation or for online parameters identification, utilize a simple PI type observer thanks to its accepted performance and simple structure. For example, in [9, 17] they have employed the PI adaptation mechanism for rotor speed, in [22] they have employed it for rotor speed and stator resistance, whereas in [19] they have employed it for rotor speed and rotor resistance. However, at very low speed region, the system noises get amplified because of the inverter nonlinearities and the use of fixed PI adaptation mechanism gains, and therefore the estimation degrades clearly and the obtained performance becomes limited [10].

In this paper, a promising solution is proposed in this case based on a fuzzy logic controller as adaptive mechanism to overcome PI controller's limitations, and then developed experimentally with a dSPACE system based on DS1104 controller board to show its effectiveness compared to a PI Luenberger observer. Also, unlike the existing schemes and to improve the performance of sensorless Indirect FOC of the induction motor drive at very low speeds, this work aims at providing simultaneous estimation of rotor speed, stator resistance and RTC inverse using the adaptive fuzzy Luenberger observer (fuzzy logic based adaptive Luenberger observer) that has been proven stable according to the Lyapunov stability theorem.

## 2 Induction Motor Model and Indirect Field Oriented Control

From the state space representation of the induction motor model in the *d-q* reference frame, the electrical equations are written as follows [13, 20]:

$$\begin{cases} \dfrac{dI_{sd}}{dt} = -\lambda I_{sd} + \omega_s I_{sq} + \dfrac{k_s}{T_s}\varphi_{rd} + \omega k_s \varphi_{rq} + \dfrac{1}{\sigma L_s} V_{sd} \\[3mm] \dfrac{dI_{sq}}{dt} = -\omega_s I_{sd} - \lambda I_{sq} - \omega k_s \varphi_{rd} + \dfrac{k_s}{T_s}\varphi_{rq} + \dfrac{1}{\sigma L_s} V_{sq} \end{cases} \quad (1)$$

$$\begin{cases} \dfrac{d\varphi_{rd}}{dt} = \dfrac{M}{T_r} I_{sd} - \dfrac{1}{T_r}\varphi_{rd} + (\omega_s - \omega)\varphi_{rq} \\[3mm] \dfrac{d\varphi_{rq}}{dt} = \dfrac{M}{T_r} I_{sq} - (\omega_s - \omega)\varphi_{rd} - \dfrac{1}{T_r}\varphi_{rq} \end{cases} \quad (2)$$

where, $(I_{sd}, I_{sq})$ and $(V_{sd}, V_{sq})$ represent, respectively the $d$-$q$ components stator currents and voltages. $(\varphi_{rd}, \varphi_{rq})$ denote the $d$-$q$ rotor components fluxes. $T_r = L_r/R_r$ and $T_s = L_s/R_s$ denote the rotor and the stator time constants, respectively.

$\omega_s$, $\omega = p\Omega$ and $\Omega$ represent respectively the synchronous, the rotor speed and the mechanical rotor speed. $L_r$ and $L_s$ are the rotor and the stator inductances, respectively. $R_r$ and $R_s$ are the rotor and the stator resistances, respectively. $M$ represent the mutual inductance and $p$ is the number of pole pairs.

And: $\sigma = 1 - \frac{M^2}{L_s L_r}; k_s = \frac{M}{\sigma L_s L_r} = \frac{1-\sigma}{M\sigma}; \lambda = \frac{1}{T_s\sigma} + \frac{1-\sigma}{T_r\sigma}$ where $\sigma$ is the blondel leakage coefficient.

The electromagnetic torque $C_e$ and the mechanical equation in the $d$-$q$ reference frame are given by:

$$C_e = p\frac{M}{L_r}(\varphi_{rd}I_{sq} - \varphi_{rq}I_{sd}) \tag{3}$$

$$\frac{d\Omega}{dt} = (C_e - C_r - f_r\Omega)/J \tag{4}$$

where, $C_r$ is the load torque, $J$ is the total inertia and $f_r$ is the friction coefficient.

The field oriented control principal consist of making the behavior of induction motor analogous to that of a DC motor in order to obtain a separation between the flux and torque by orienting the '$d$' axis along the rotor flux axis as shown in Fig. 1. Under this condition we get [4, 16]:

$$\varphi_{rd} = \varphi_r, \varphi_{rq} = 0 \tag{5}$$

where $\varphi_r$ is the total rotor flux.

By using Eq. (5) in Eq. (1), we get:

$$\begin{cases} V_{sd} = \sigma L_s\frac{dI_{sd}}{dt} + \lambda\sigma L_s I_{sd} - \sigma L_s\omega_s I_{sq} - \sigma L_s\frac{k_s}{T_s}\varphi_r \\ V_{sq} = \sigma L_s\frac{dI_{sq}}{dt} + \lambda\sigma L_s I_{sq} + \sigma L_s\omega_s I_{sd} + \sigma L_s\omega k_s\varphi_r \end{cases} \tag{6}$$

$$a_1 = -\lambda; \; a_2 = \frac{k_s}{T_r}; \; a_3 = k_s; \; a_4 = \frac{M}{T_r}; \; a_5 = -\frac{1}{T_r}; \; a_6 = \frac{1}{\sigma L_s}; \; a_7 = \frac{1-\sigma}{\sigma}; \; \beta_r = \frac{1}{T_r}$$
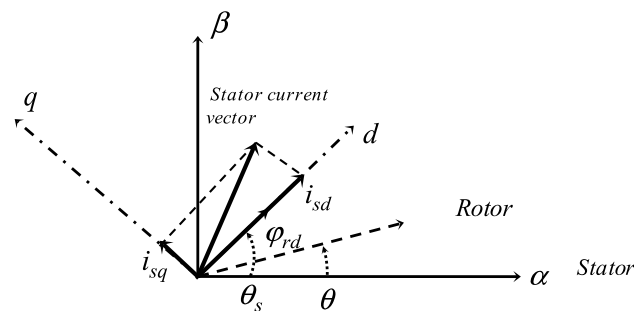
From Eq. (6), it can be seen that both currents components $(I_{sd}, I_{sq})$ are controlled by voltages $(V_{sd}, V_{sq})$ and then acts on flux and torque. In this case, it is required to ensure a decoupling by introducing compensation terms $E_d$ and $E_q$.

Where:

$$\begin{cases} E_d = \sigma L_s\omega_s I_{sq} + \sigma L_s\frac{k_s}{T_s}\varphi_r \\ E_q = -\sigma L_s\omega_s I_{sd} - \sigma L_s\omega k_s\varphi_r \end{cases} \tag{7}$$

Equation (6) becomes:

$$\begin{cases} V_{sd} = V'_{sd} - E_d \\ V_{sq} = V'_{sq} - E_q \end{cases} \tag{8}$$

A new system of equations is obtained:

$$\begin{cases} V'_{sd} = \sigma L_s\frac{dI_{sd}}{dt} + \lambda\sigma L_s I_{sd} \\ V'_{sq} = \sigma L_s\frac{dI_{sq}}{dt} + \lambda\sigma L_s I_{sq} \end{cases} \tag{9}$$

Furthermore, the torque expression becomes:

$$C_e = p\frac{M}{L_r}\varphi_r I_{sq} \tag{10}$$

By using Eq. (5) in Eq. (2), we get:

$$\begin{cases} \varphi_r = MI_{sd} \quad (*) \\ (\omega_s - \omega) = \frac{MI_{sq}}{T_r\varphi_r} = \omega_r \quad (**) \end{cases} \tag{11}$$

where $\omega_r$ is the slip speed.

Finally, by using the expression of $\varphi_r$ (*) in (**) and integrating (**), we get:

$$\theta_s = \int\left(\frac{I_{sq}}{T_r I_{sd}} + \theta\right)dt \tag{12}$$

where, $\theta_s$ and $\theta$ are the position of the $d$-$q$ reference frame and the rotor position, respectively. Later in this article, the following notations will be used:



Fig. 1 Principle of the vector control

## 3 Sensorless Indirect FOC Using the Improved Luenberger Observer

The mathematical model of the induction motor in the stationary reference frame $\alpha$-$\beta$ using state space representation is described by the following equations [19]:
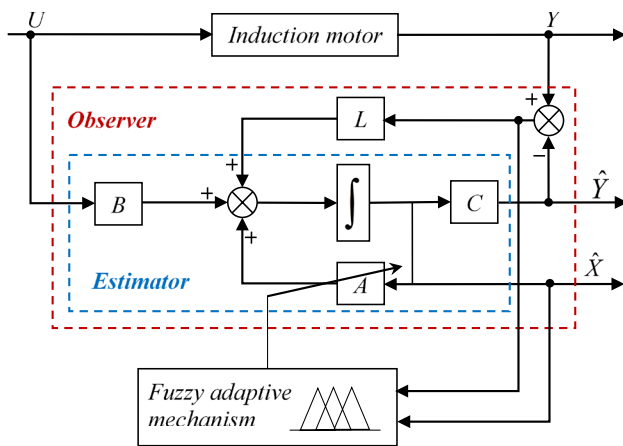
**Fig. 2** The adaptive Luenberger observer Structure

$$\dot{X} = A(\omega, R_s, \beta_r)X + BU$$
$$Y = CX \tag{13}$$

where,

$$A(\omega, R_s, \beta_r) = \begin{bmatrix} -R_s a_6 - \beta_r a_7 & 0 & \beta_r a_3 & \omega a_3 \\ 0 & -R_s a_6 - \beta_r a_7 & -\omega a_3 & \beta_r a_3 \\ M\beta_r & 0 & -\beta_r & -\omega \\ 0 & M\beta_r & \omega & -\beta_r \end{bmatrix},$$

$$B = \begin{bmatrix} 1/\sigma L_s & 0 \\ 0 & 1/\sigma L_s \\ 0 & 0 \\ 0 & 0 \end{bmatrix}, C = \begin{bmatrix} 1 & 0 & 0 & 0 \\ 0 & 1 & 0 & 0 \end{bmatrix}, X = \begin{bmatrix} I_{s\alpha} \\ I_{s\beta} \\ \varphi_{r\alpha} \\ \varphi_{r\beta} \end{bmatrix}, U = \begin{bmatrix} V_{s\alpha} \\ V_{s\beta} \end{bmatrix}, Y = \begin{bmatrix} I_{s\alpha} \\ I_{s\beta} \end{bmatrix} \tag{14}$$

And $(V_{s\alpha}, V_{s\beta})$ and $(I_{s\alpha}, I_{s\beta})$ represent the $\alpha$-$\beta$ stator voltages and currents components, respectively. $(\varphi_{r\alpha}, \varphi_{r\beta})$ are the $\alpha$-$\beta$ rotor fluxes components.

### 3.1 Luenberger Observer Structure

In this work, the adaptive Luenberger observer is a state observer estimating the induced fluxes, the stator currents and the other parameters (rotor speed, stator resistance and RTC inverse). These latter which constitute the output of the fuzzy adaptive mechanisms are estimated to be used for the tuning in the state matrix as shown in Fig. 2 and/or for feedback in the case of the estimated speed. The structure of the proposed observer is depicted in Fig. 2 whereas the overall block diagram of sensorless indirect FOC for induction motor drive using the adaptive fuzzy Luenberger observer is depicted in Fig. 3.

The main components of this sensorless vector control are the adaptive fuzzy Luenberger observer, the speed control loop (an outer loop), the $I_{sd}$ and $I_{sq}$ currents control loops (inner loops), $\theta_s$ calculation block and the direct and inverse Park transformations. The input of the speed control loop is the reference speed $\Omega^*$. This latter is compared

to the estimated speed $\hat{\Omega}$ provided by the adaptive fuzzy Luenberger observer whose inputs are the measured stator currents and the reference stator voltages. The speed control error $(\Omega^* - \hat{\Omega})$ represents the input of the speed controller whose output is the reference torque given by $C_e^*$ which provides the reference current $I_{sq}^*$, obtained from Eq. (10). This latter, is compared to the measured current $I_{sq}$ given by the current sensor. The current control error $(I_{sq}^* - I_{sq})$ represents the input of the Q-axis current controller whose output is the reference voltage $V_{sq}^*$. In parallel with this inner $I_{sq}$ control loop, we find another $I_{sd}$ control loop. The reference current $I_{sd}^*$, obtained from equation Eq. (11) is compared to the measured current $I_{sd}$ given by the current sensor. The current control error $(I_{sd}^* - I_{sd})$ represents the input of the D-axis current controller whose output is the reference voltage $V_{sd}^*$. Both reference voltages $V_{sd}^*$ and $V_{sq}^*$ are transformed to three-phase quantities $(V_{sa}^*, V_{sb}^*, V_{sc}^*)$ using the position $\theta_s$ obtained from the estimated rotor speed and the slip speed given by Eq. (11). These reference voltages are considered

as the input of the PWM (Pulse Width Modulation) blocks which drive the voltage source inverter.

The superscript '^' represents estimated quantities and the superscript '*' represents references of the quantities.

The Luenberger observer equations are given by [19]:

$$\dot{\hat{X}} = A(\hat{\omega}, \hat{R}_s, \hat{\beta}_r)\hat{X} + BU + L(Y - \hat{Y})$$
$$\hat{Y} = C\hat{X} \tag{15}$$

where

$$\hat{X} = \begin{bmatrix} \hat{I}_{s\alpha} \\ \hat{I}_{s\beta} \\ \hat{\varphi}_{r\alpha} \\ \hat{\varphi}_{r\beta} \end{bmatrix}, \hat{Y} = \begin{bmatrix} \hat{I}_{s\alpha} \\ \hat{I}_{s\beta} \end{bmatrix}, A(\hat{\omega}, \hat{R}_s, \hat{\beta}_r)$$

$$= \begin{bmatrix} -\hat{R}_s a_6 - \hat{\beta}_r a_7 & 0 & \hat{\beta}_r a_3 & \hat{\omega} a_3 \\ 0 & -\hat{R}_s a_6 - \hat{\beta}_r a_7 & -\hat{\omega} a_3 & \hat{\beta}_r a_3 \\ M\hat{\beta}_r & 0 & -\hat{\beta}_r & -\hat{\omega} \\ 0 & M\hat{\beta}_r & \hat{\omega} & -\hat{\beta}_r \end{bmatrix} \tag{16}$$
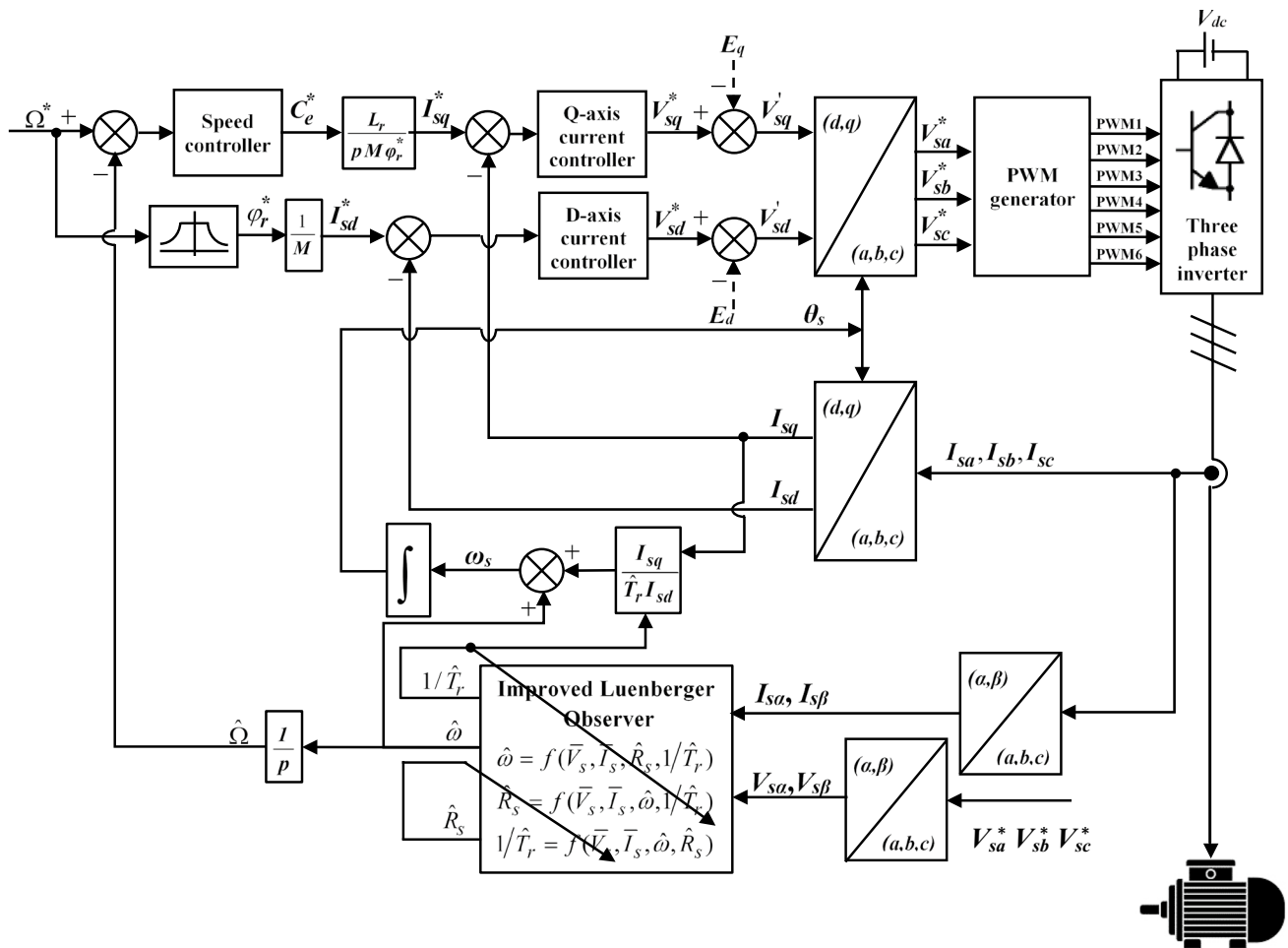
We put:

**Fig. 3** Sensorless indirect FOC block diagram using the adaptive fuzzy Luenberger observer with online parameters identification

$$A' = A(\hat{\omega}, \hat{R}_s, \hat{\beta}_r) - LC \tag{17}$$

Equation (15) becomes:

$$\hat{X} = A(\hat{\omega}, \hat{R}_s, \hat{\beta}_r)\hat{X} + BU + LY - LC\hat{X} = A'\hat{X} + BU + LY \tag{18}$$

The stator current and the rotor flux estimation error is given by the following equation:

$$e = X - \hat{X} = \begin{bmatrix} e_{I_{s\alpha}} \\ e_{I_{s\beta}} \\ e_{\varphi_{r\alpha}} \\ e_{\varphi_{r\beta}} \end{bmatrix} = \begin{bmatrix} I_{s\alpha} - \hat{I}_{s\alpha} \\ I_{s\beta} - \hat{I}_{s\beta} \\ \varphi_{r\alpha} - \hat{\varphi}_{r\alpha} \\ \varphi_{r\beta} - \hat{\varphi}_{r\beta} \end{bmatrix} \tag{19}$$

By deriving Eq. (19), we obtain the following equation:

$$\dot{e} = \dot{X} - \dot{\hat{X}} \tag{20}$$

We then replace $\dot{X}$ and $\dot{\hat{X}}$ by their expressions from equations Eq. (13) and Eq. (15) and we add and subtract the quantity $A'X$ to get:

$$\begin{aligned} \dot{e} &= \left(A(\omega, R_s, \beta_r)X + BU\right) - \left(A'\hat{X} + BU + LY\right) \\ &= A(\omega, R_s, \beta_r)X - A'\hat{X} - LY + A'X - A'X \end{aligned} \tag{21}$$

By using Eq. (19) and by replacing $A'$ by its expressions (as expressed in Eq. (17)), we get:

$$\dot{e} = A(\omega, R_s, \beta_r)X - LY + A'e - \left(A(\hat{\omega}, \hat{R}_s, \hat{\beta}_r) - LC\right)X \tag{22}$$

We finally obtain the expression of the error derivative:

$$\dot{e} = A'e - \Delta A\hat{X} \tag{23}$$

where, $\Delta A = A(\omega, R_s, \beta_r) - A(\hat{\omega}, \hat{R}_s, \hat{\beta}_r) =$
$$\begin{bmatrix} -\Delta R_s a_6 - \Delta\beta_r a_9 & 0 & \Delta\beta_r a_3 & \Delta\omega\, a_3 \\ 0 & -\Delta R_s a_6 - \Delta\beta_r a_9 & -\Delta\omega\, a_3 & \Delta\beta_r a_3 \\ M\Delta\beta_r & 0 & -\Delta\beta_r & -\Delta\omega \\ 0 & M\Delta\beta_r & \Delta\omega & -\Delta\beta_r \end{bmatrix}.$$
And $\Delta\omega = \omega - \hat{\omega}$; $\Delta R_s = R_s - \hat{R}_s$; $\Delta\beta_r = \beta_r - \hat{\beta}_r$.

For observer gain matrix $L$ determination, conventional pole placement technique will be used:

In order to guarantee the system stability and to improve its transient response, the eigenvalues of the matrix $A'$ are placed in the left half of the complex plane. Thus, as presented in [17], the observer gain matrix $L$ is calculated so that the observer poles are proportional to those of the induction motor (proportional constant $k > 1$).

This means that the eigenvalues of full order Luenberger observer ($\lambda_{LO}$) and the IM ($\lambda_{IM}$) must be satisfied using the following equation:

$$\lambda_{LO} = k\lambda_{IM} \tag{24}$$

The eigenvalues of the full order Luenberger observer can be calculated using the following equation:

$$\det\left(\lambda_{LO} I_4 - A\left(\hat{\omega}, \hat{R}_s, \hat{\beta}_r\right) + LC\right) = 0 \tag{25}$$

where, $I_4$ is the $(4 \times 4)$ identity matrix.

Whereas the eigenvalues of the induction motor can be calculated using the following equation:

$$\det\left(\lambda_{IM} I_4 - A\left(\omega, R_s, \beta_r\right)\right) = 0 \tag{26}$$

The observer gain matrix can be considered as follows:

$$L = \begin{bmatrix} l_1 & l_2 & l_3 & l_4 \\ -l_2 & l_1 & -l_4 & l_3 \end{bmatrix}^T, \tag{27}$$

The feedback gains are designed as follow:

$$\begin{cases} l_1 = -(k-1)(a_1 + a_5) \\ l_2 = -(k-1)\omega \\ l_3 = (k^2 - 1)\left(\dfrac{a_1}{a_3} - a_4\right) - \dfrac{1}{a_3}(k-1)(a_1 + a_5) \\ l_4 = -\dfrac{1}{a_3}(k-1)\omega \end{cases} \tag{28}$$

Figures 4a, b illustrate the motor and the observer poles trajectories (considering different values of the constant $k$) respectively. The speed ranges from $-140$ to $140$ rad/s. As shown in Fig. 4b, the constant $k$ should not be very large in order not to destabilize the system.

## 3.2 Rotor Speed, Stator Resistance and RTC Inverse Estimation Using the Adaptive fuzzy Luenberger Observer

The adaptive LO will be proved stable according to the Lyapunov method. In our case, the Lyapunov function candidate is defined as follow:

$$V = e^T e + \frac{\Delta\omega^2}{\delta_\omega} + \frac{\Delta R_s^2}{\delta_{R_s}} + \frac{\Delta\beta_r^2}{\delta_{\beta_r}} \tag{29}$$

where, $\delta_\omega, \delta_{R_s}$ and $\delta_{\beta_r}$ are positive constants.

To satisfy the sufficient condition of the uniform asymptotic stability, the time derivative of the Lyapunov function should be negative definite [18]. $\dot{V}$ is defined as:
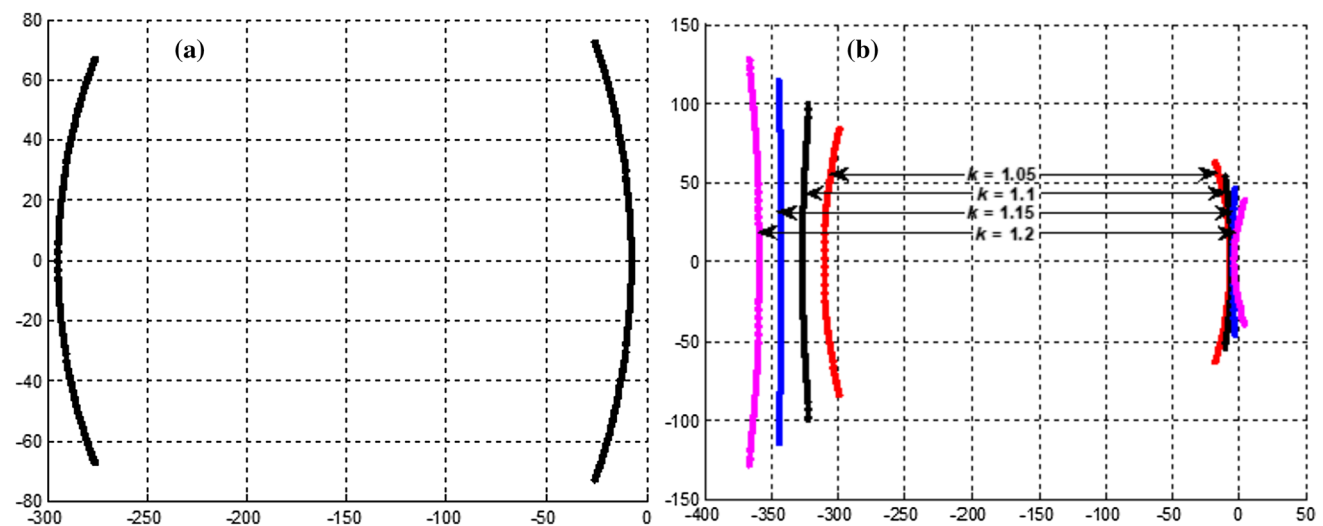


Fig. 4 a The IM poles trajectory for variable motor speeds; b the observer poles trajectory for variable motor speeds and for different values of '$k$'

$$\frac{dV}{dt} = \frac{de^T}{dt}e + e^T\frac{de}{dt} + \frac{1}{\delta_\omega}\frac{d(\Delta\omega^2)}{dt} + \frac{1}{\delta_{R_s}}\frac{d(\Delta R_s^2)}{dt} + \frac{1}{\delta_{\beta_r}}\frac{d(\Delta\beta_r^2)}{dt} \tag{30}$$

For the derivation of the adaptive mechanism, the parameters $\omega$, $R_s$ and $\beta_r$ are considered constant [17]. The expression of $\dot{V}$ becomes:

$$\frac{dV}{dt} = +2\Delta\omega\, a_3\left(\hat{\varphi}_{r\beta}\, e_{I_{s\alpha}} - \hat{\varphi}_{r\alpha}\, e_{I_{s\beta}}\right) - 2\frac{1}{\delta_\omega}\Delta\omega\frac{d(\hat{\omega})}{dt} + e^T\left[(A')^T + A'\right]e$$

$$+2\Delta\beta_r\left(a_3\hat{\varphi}_{r\alpha}\, e_{I_{s\alpha}} + a_3\hat{\varphi}_{r\beta}\, e_{I_{s\beta}} - a_7\hat{I}_{s\alpha}\, e_{I_{s\alpha}} - a_7\hat{I}_{s\beta}\, e_{I_{s\beta}}\right) - 2\frac{1}{\delta_{\beta_r}}\Delta\beta_r\frac{d(\hat{\beta}_r)}{dt}$$

$$-2a_6\Delta R_s\left(\hat{I}_{s\alpha}\, e_{I_{s\alpha}} + \hat{I}_{s\beta}\, e_{I_{s\beta}}\right) - 2\frac{1}{\delta_{R_s}}\Delta R_s\frac{d(\hat{R}_s)}{dt} + 2\Delta\omega\left(\hat{\varphi}_{r\alpha}\, e_{\varphi_{r\beta}} - \hat{\varphi}_{r\beta}\, e_{\varphi_{r\alpha}}\right)$$

$$+2M\,\Delta\beta_r\left(\hat{I}_{s\alpha}\, e_{\varphi_{r\alpha}} + \hat{I}_{s\beta}\, e_{\varphi_{r\beta}}\right) - 2\Delta\beta_r\left(\hat{\varphi}_{r\alpha}\, e_{\varphi_{r\alpha}} + \hat{\varphi}_{r\beta}\, e_{\varphi_{r\alpha}}\right) \tag{31}$$

In order to satisfy the observer stability using Lyapunov criteria, the time derivative has to be negative. The term: $e^T([(A')^T + (A')])e$ is negative, because of the imposed eigenvalues of the observer whereas terms multiplied by the fluxes estimation errors $e_{\varphi_{r\alpha}}$ and $e_{\varphi_{r\beta}}$ are neglected if we suppose that in vector control these errors are very small.

The rest of the quantities can be set to values less than zero or equal to zero:

$$+2\Delta\omega a_3 e_\omega - 2\frac{1}{\delta_\omega}\Delta\omega\frac{d(\hat{\omega})}{dt} = 0, \quad -2\Delta R_s a_6 e_{R_s} - 2\frac{1}{\delta_{R_s}}\Delta R_s\frac{d(\hat{R}_s)}{dt} = 0$$

$$+2\Delta\beta_r e_{\beta_r} - 2\frac{1}{\delta_{\beta_r}}\Delta\beta_r\frac{d(\hat{\beta}_r)}{dt} = 0 \tag{32}$$

where,

$$e_\omega = \left(\hat{\varphi}_{r\beta}\, e_{I_{s\alpha}} - \hat{\varphi}_{r\alpha}\, e_{I_{s\beta}}\right), \quad e_{R_s} = \left(\hat{I}_{s\alpha}\, e_{I_{s\alpha}} + \hat{I}_{s\beta}\, e_{I_{s\beta}}\right),$$

$$e_{\beta_r} = \left(a_3\hat{\varphi}_{r\alpha}\, e_{I_{s\alpha}} + a_3\hat{\varphi}_{r\beta}\, e_{I_{s\beta}} - a_7\hat{I}_{s\alpha}\, e_{I_{s\alpha}} - a_7\hat{I}_{s\beta}\, e_{I_{s\beta}}\right) \tag{33}$$

Finally, we get:

$$\hat{\omega} = \delta_\omega a_3\int e_\omega dt, \qquad \hat{R}_s = -\delta_{R_s}a_6\int e_{R_s}dt, \qquad \hat{\beta}_r = \delta_{\beta_r}\int e_{\beta_r}dt \tag{34}$$

Fuzzy logic that was originally developed by Lotfi Zadeh in 1965 [37], has been exploited successfully in several areas and utilized to solve many complex problems related to complex control of nonlinear and time varying parameters models. In the case of the IM, fuzzy logic techniques have been proposed for error minimization in different applications, such as, speed control, switching table of DTC and online tuning of the speed and/or the motor parameters [1, 5, 10, 20, 31, 34]. In this proposed Luenberger observer, fuzzy logic has been introduced as an adaptive mechanism to generate the speed and the other parameters from the errors (whose expressions are listed in Eq. (33)) and their derivatives.

As shown in Fig. 5, the fuzzy logic block is composed of three main blocks: Fuzzification, inference mechanism (rules base), and defuzzification. Figure 6 shows the input signals: $er$ and its derivative $\dot{er}$ and the output signal: $\hat{x}$ membership functions.

The choice of the range (universe of discourse) of the membership functions variations is generally related to the nature of the input variables. In this article, we aim to improve the rotor speed and the parameters estimation using fuzzy logic based adaptive Luenberger observer (FL based ALO).

The input of the FL block is an error for which we have imposed this range [−0.1, 0.1]. Thereafter, in order to have high performances of the observer, two adjustment gains $K_1$ and $K_2$ have been added in order to normalize the input quantities to always get the suitable weights of the membership functions.

Only three membership functions (triangular functions) that have been used for inputs and for output of the Fuzzy Logic block in order to simplify the practical implementation and in order to reduce execution time and algorithm complexity. In addition, through simulation tests, we noticed that the use of more than three membership function does not make a significant improvement to the system performances [20]. Therefore, the Fuzzy logic block has nine fuzzy IF–THEN rules as shown in Table 1. Where, N means Negative, Z means Zero and P means Positive. Defuzzification is done by centroid method based on the inference method Mamdani for more precision. All gains used in this sensorless drive are shown in Table 2.
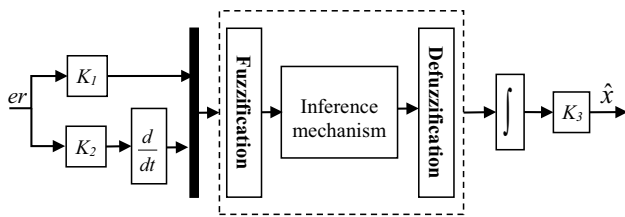
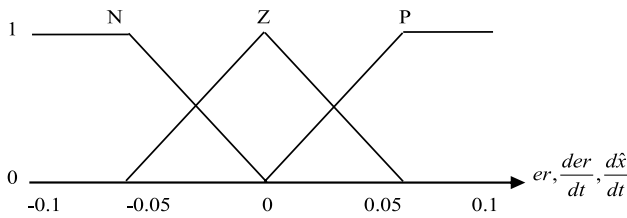**Fig. 5** Internal structure of the fuzzy logic controller



**Fig. 6** Inputs and output membership functions of the fuzzy logic controller

**Table 1** The fuzzy adaptation mechanism rules base

| $er/\dot{e}r$ | N | Z | P |
|---|---|---|---|
| N | N | N | Z |
| Z | N | Z | P |
| P | Z | P | P |

**Table 2** Gains of Controllers Used for Estimation

| Gains of the fuzzy controller | | Gains of the PI controller | |
|---|---|---|---|
| $K_{1\omega}$, $K_{2\omega}$ and $K_{3\omega}$ | 14, 0.5, 200 | $K_{p\omega}$ and $K_{i\omega}$ | 10, 900 |
| $K_{1Rs}$, $K_{2Rs}$ and $K_{3Rs}$ | 10, 0.05, 20 | $K_{pRs}$ and $K_{iRs}$ | 1, 100 |
| $K_{1\beta r}$, $K_{2\beta r}$ and $K_{3\beta r}$ | 3, 3, 30 | $K_{p\beta r}$ and $K_{i\beta r}$ | 0.5, 5 |

# 4 Experimental Results and Discussions

The proposed sensorless IFOC of the induction motor drive using the Adaptive Fuzzy Luenberger Observer has been validated. The scheme shown in Fig. 3 has been used for experimental tests. The overview of the experimental setup shown in Fig. 7 consists of: (i) An Industrial IGBTs Voltage Source Inverter (VSI) from SEMIKRON connected to a DC voltage of 400 V, with a gate driver circuit SKHI-20opA and two current sensors LEM 55-P. (ii) A dSPACE 1104 board with a 250 MHz 603-PowerPC processor and a slave-DSP based on 20 MHz TMS320F240 DSP from Texas Instrument used for PWM signals generation. In addition to DS1104_ADC converters with a resolution of 12 bits and a conversion time of 800 ns with a full-scale input voltage of ± 10 V. These latter were used for currents and speed acquisition. In fact, measurements obtained from currents sensors are converted to voltages ranging from 0 to ± 10 V before connection to the DS1104_ADC converters. Regarding the stator voltages, we used the reference stator voltages available in the algorithm to avoid the measurement of the high-frequency PWM stator voltages. (iii) A dSPACE panel serving as interface between the output sensor and the inputs of the dSPACE 1104 board (iv) A squirrel cage Induction Motor of 1 kW is used with parameters listed in Table 3. Load torque is adjusted by changing external resistances through a DC generator coupled to the induction motor. (v) A tachometer (20 V for 1000 rpm) is used to provide the real motor speed for comparison with its estimated value.

The tight integration of dSPACE software with MATLAB/Simulink®, which is a common engineering software, provides a powerful development environment. Indeed, according to Fig. 8, the six PWM TTL-signals are generated based on Simulink real-time blocks including the DS1104SL_DSP_PWM3 unit whose inputs are the reference voltages. To generate the real time C code, the Simulink file is built with the help of Real-Time Workshop (RTW) and Real Time Interface (RTI), and then downloaded on the 32 MB dSPACE memory. In order to ensure an optimal execution of the all parts of the sensorless drive, especially PWM generation and currents measurements, the PWM frequency was chosen equal to 6 kHz and the sampling time is equal to 100 μs.

For real time monitoring, the dSPACE board is used with Control Desk software which makes easy data processing and visualization.

To show the validity and the effectiveness of the proposed IFOC sensorless drive, experimental tests were done in wide ranges of speed under load and no load especially at low and zero speed operations.

The experimental results are illustrated with relevant discussions in the following subsections.

The errors expressions are as follows: $e_{FL} = \Omega - \hat{\Omega}_{FL}$ and $e_{PI} = \Omega - \hat{\Omega}_{PI}$. Where, $\hat{\Omega}_{FL}$ and $\hat{\Omega}_{PI}$ are the estimated speed using the FL based ALO and PI based ALO, respectivly.

## 4.1 Open-Loop Comparison of the Estimated Speed Using PI and Fuzzy LO

The actual rotor speed and the estimated speeds obtained with PI and fuzzy adaptive scheme are presented in Fig. 9. For better comparison between the two adaptation mechanisms (FL and PI controllers respectively) speed estimation errors are observed in Fig. 10.

In order to illustrate performance of the adaptive mechanism, an open loop test is mandatory when the IFOC control uses the actual speed as feedback signal. Also, in the comparative study of this paper, the main focus is on the operation of the speed estimators at low speeds due to poor operation of estimators in this region.
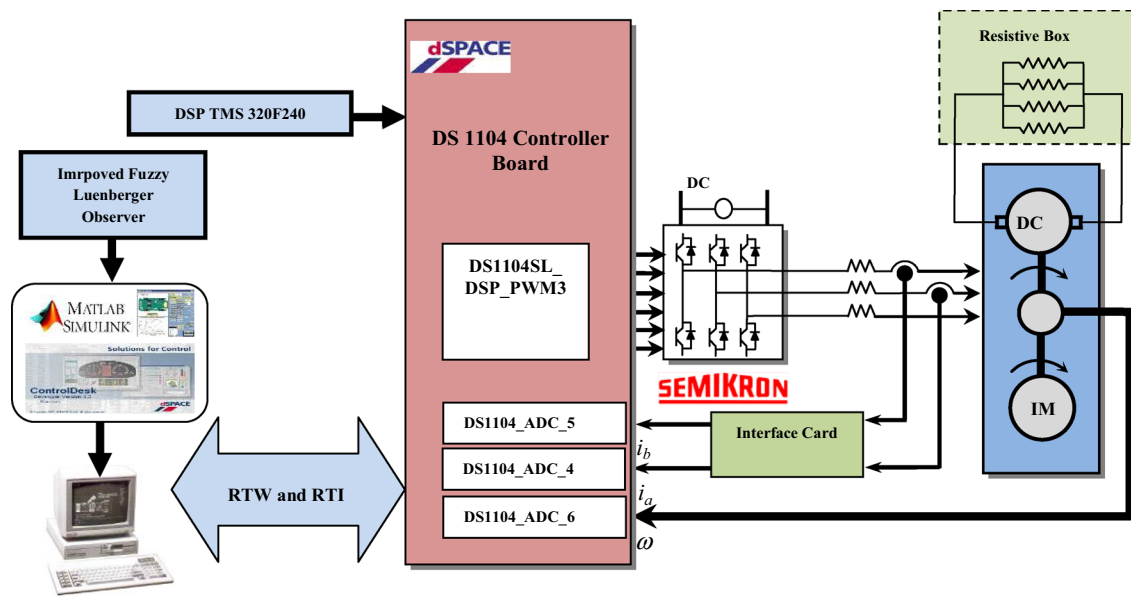
**Fig. 7** Block diagram of the experimental test bench

**Table 3** Motor Specifications and Parameters

| Motor specifications | | Motor parameters |
|---|---|---|
| Rated power | 1 kW | $L_s = 0.3973$ H; |
| Rated current | 2.65 A | $L_r = 0.3558$ H; |
| Rated frequency | 50 Hz | $M = 0.35$ H; |
| Rated speed | 1425 rpm | $R_s = 6.8\ \Omega$; |
| Rated voltage | 400 V | $R_r = 5.43\ \Omega$; |
| Number of pole pairs | $p = 2$ | $f_r = 0.0025$ Nm.s.rad$^{-1}$; $J = 0.02$ kg.m$^2$ |

In the case of zero and low speed test as shown in Fig. 9(b), by comparing speed estimation errors in Fig. 10(b), it is completely clear that the PI controller has significant error especially at zero speed. From Figs. 9a and 10a, comparison between the operation of PI and fuzzy adaptive schemes from low to high speed tests confirm that fuzzy logic controller has better transient and steady-state behavior.

## 4.2 Rated Speed Response of the Drive

The performances of the sensorless drive (without stator resistance and RTC estimation) obtained with the PI based Adaptive Luenberger Observer and the proposed Fuzzy Logic based Adaptive Luenberger Observer are shown in Fig. 11. They show sensorless IM drive when different ranges of speed references are applied at no load with different speed reference profiles. Set of speed reference variations are applied from low to high speed

$(100 \rightarrow 600 \rightarrow 1100 \rightarrow 1425)$ then a ramp speed command is applied from rated speed to low speed (100 rpm). In these tests, estimated speed is used as feedback in order to ensure a closed-loop control. Results show good tracking performance of the estimated speed at both transient and steady states. The speed estimation errors are given in Fig. 12 for comparison. We can observe that the speed estimation error with the PI based ALO is more important than the speed estimation error with FL based ALO especially in the case when the induction motor is running at high speed and not loaded.

## 4.3 Low and Zero Speed Performance of the Drive

Sensorless speed control experimental results are presented here at − 100 rpm (reverse direction) then zero speed then 100 rpm reference. Figures 13 and 14 present the reference, the real and the estimated speeds using the FL based ALO and the PI based ALO, whereas Figs. 15 and 16 represent the speed estimation errors. It can be noticed that around zero speed the actual speed and the estimated speed does not fit the speed reference because of the reference voltages (used as inputs of the adaptive Luenberger observer) that deviate substantially from the actual motor voltages. This problem which remains a challenge is caused by the inverter dead time effects and inverter nonlinearities. However, the estimated speed using FL based LO remains close to the reference speed and less undulated at very low speeds compared to the one obtained with the PI based ALO.

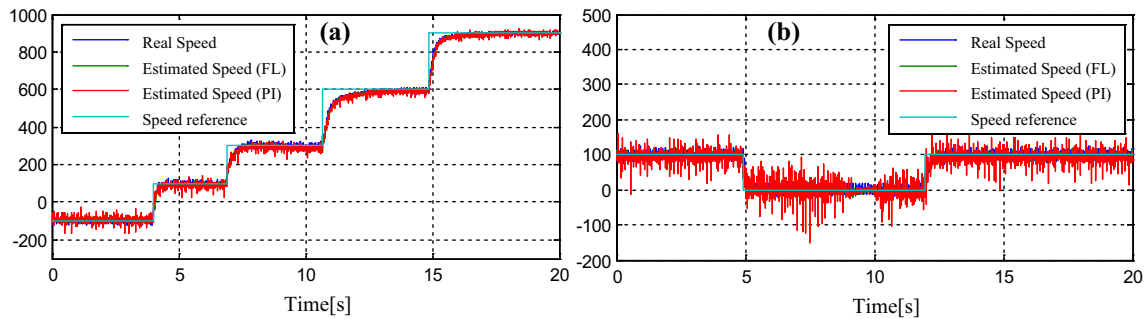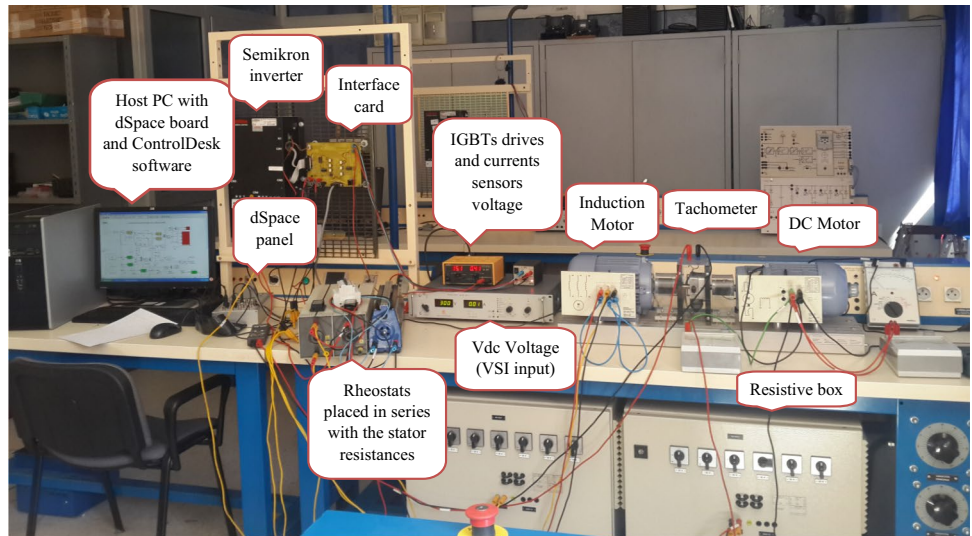**Fig. 8** Photograph of the experimental setup



**Fig. 9** Actual and the estimated speeds responses with (PI Vs FL) Luenberger observer: **a** Step speed variations: from − 100 to 900 rpm; **b** Step speed variations: 100→0→100 rpm
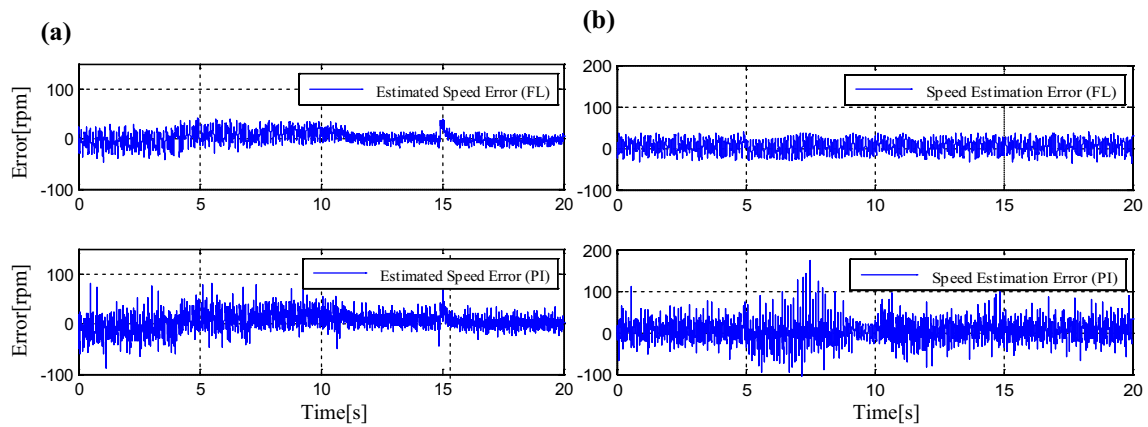


**Fig. 10** Speed estimation errors **a** speed: from − 100 to 900 rpm; **b** speed: 100→0→100 rpm

## 4.4 Effect of Loading

The induction motor is running at 700 rpm with 2.75 N.m load when step reference of 300 rpm is introduced. The loading performances of the sensorless drives are observed in Figs. 17, 18 and 19. The induction motor is operated at 1000 rpm when a load torque of 1 N.m is introduced at 13.5 s/11.5 s to reach 3.75 N.m then withdrawn at 20.5 s. As one can see in Fig. 17, the estimated speeds follow the real speed in both transient and steady states, the undershoot and the overshoot appear in the real and estimated speed during load torque introduction and removal. However, Fig. 17a shows that the rotor speed estimated with FL based ALO is less undulated than the one obtained with the PI based ALO.

As shown in Fig. 18, the speed estimation error remains negligible using FL based ALO. The profiles of the electromagnetic torques are shown in Fig. 19, as shown it is obvious the increase of the torque ripples with the PI based ALO.

## 4.5 Responses of the Estimated RTC Inverse and Stator Resistance

In the rest of the tests, the rotor speed, the inverse of the RTC and the stator resistance are estimated simultaneously.

In order to observe the stator resistance effect on the estimated and the real speeds, three rheostats in parallel with three phase circuit breaker have been put in series with the IM stator resistances as shown in Figs. 7 and 8. The stator resistances value is increased sharply at 4 s by 5.5 Ω to reach 12 Ω and decreased sharply by 5.5 Ω after some few seconds. It can be noticed that the estimated resistance follows the real one as shown in Fig. 21.

The estimated RTC inverse is used as input of the adaptive fuzzy Luenberger observer for both rotor speed and stator resistance estimation according to the adaptive model equations (the same for the stator resistance and the rotor speed). From Eq. (11) and as illustrated in Fig. 3, the RTC inverse is also used in slip speed expression. Figure 22 shows then a good convergence of $\beta_r$.

On the other hand, as observed in Figs. 20a, 21a, 22a, the experimental results clearly highlight and demonstrate the efficiency of the proposed adaptive fuzzy Luenberger observer compared to the PI based ALO.

We can observe that the FL based ALO has brought significant improvement to the PI based ALO by reducing clearly oscillations and ripples in all estimated quantities. This improvement is obtained even when the rotor speed and the other parameters are estimated simultaneously in
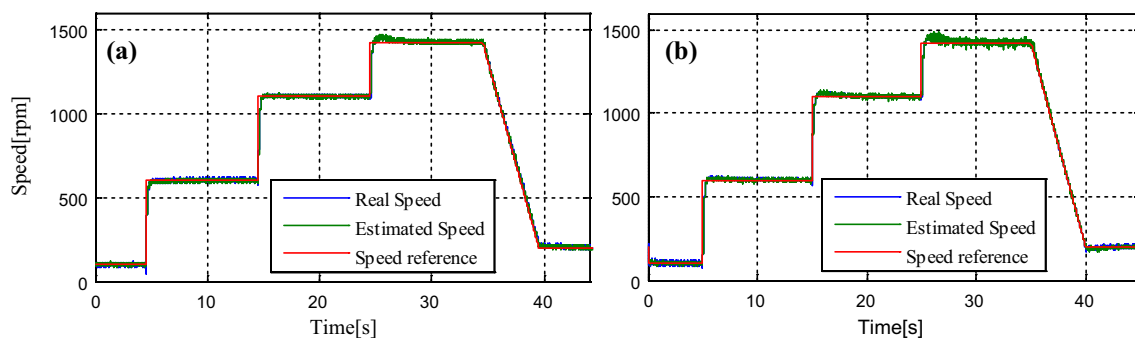


**Fig. 11** Step speed responses from low to rated speed (off load) using: **a** FL based ALO, **b** PI based ALO
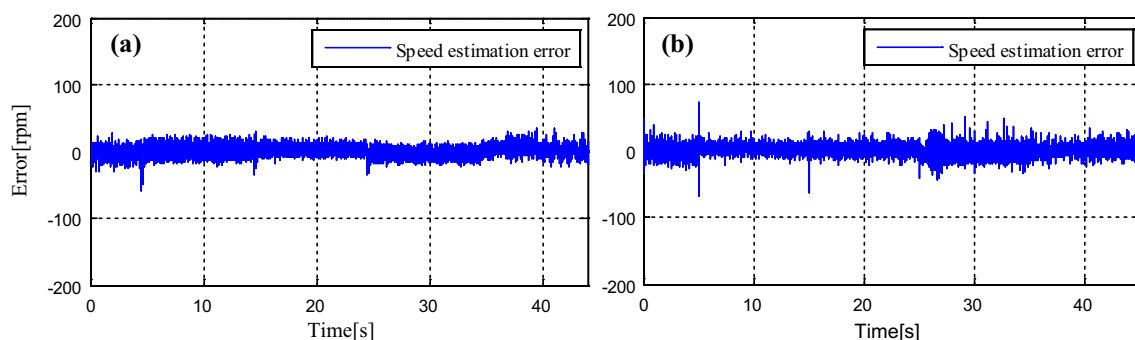


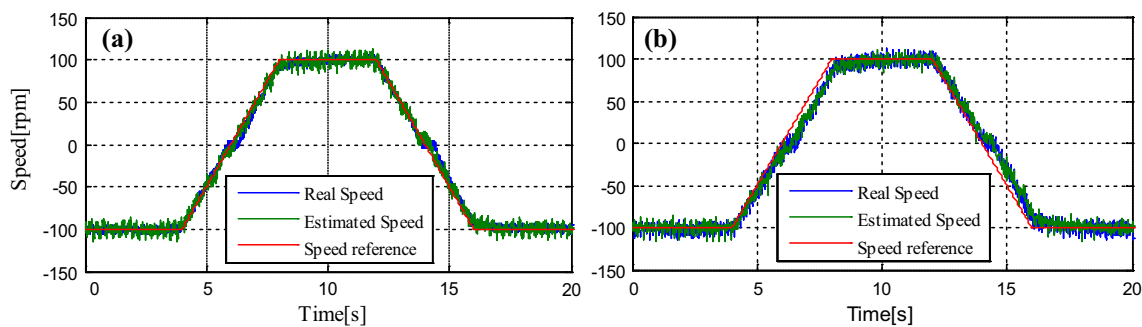**Fig. 12** Speed estimation errors: **a** FL based ALO, **b** PI based ALO

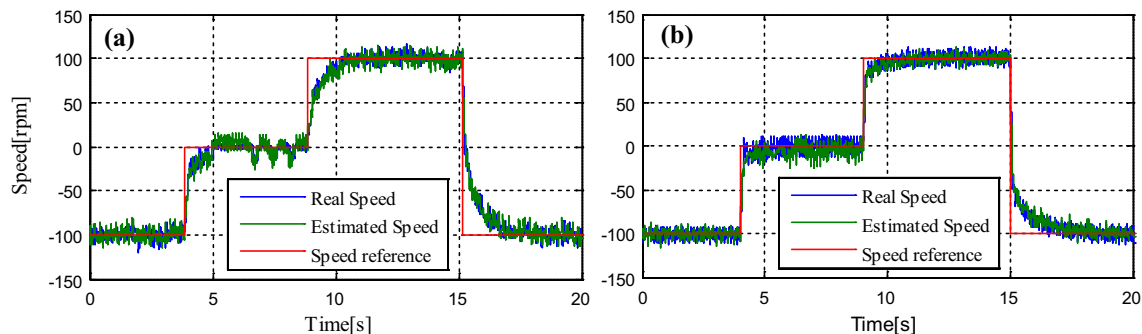**Fig. 13** Ramp speed responses (off load) using: **a** FL based ALO, **b** PI based ALO



**Fig. 14** Step speed responses at low speeds (off load) using: **a** FL based ALO, **b** PI based ALO
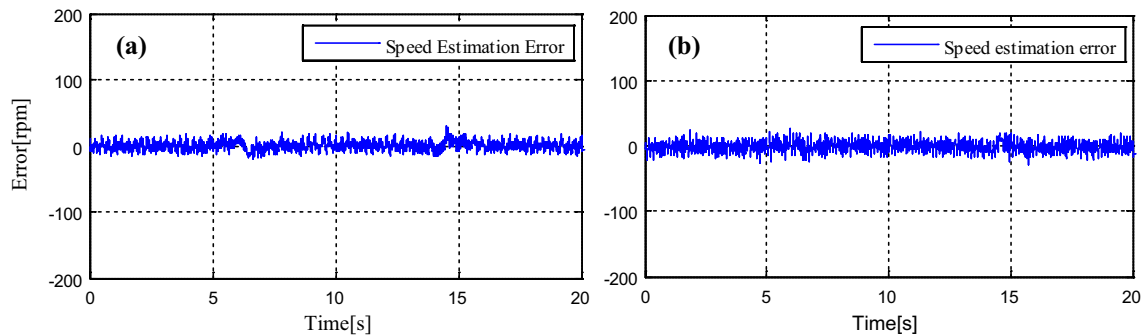


**Fig. 15** Speed estimation errors: **a** FL based ALO, **b** PI based ALO

the presence of stator resistance variation (when its value has increased by more than 25% from its nominal value).

### 4.6 Parameters Identification at Very Low Speeds

The motor speed is changed from 45 rpm to − 45 rpm then from − 45 rpm to 45 rpm as shown in Fig. 23. The test objective is to show performances of the proposed sensorless drive with parallel parameters identification at very low speeds in both directions of rotation.

In particular, Figs. 23 and 24 show very satisfying performances obtained at very low speeds with no-load torque since the effect of the inverter nonlinearities has been eliminated using FL based ALO.

Furthermore, the experimental results show that the estimated parameters obtained with FL based ALO are slightly affected by the speed variation compared to the ones obtained with the PI based ALO as shown in Figs. 25b, 26b, especially at zero crossing (at 2.5 s and 13 s).
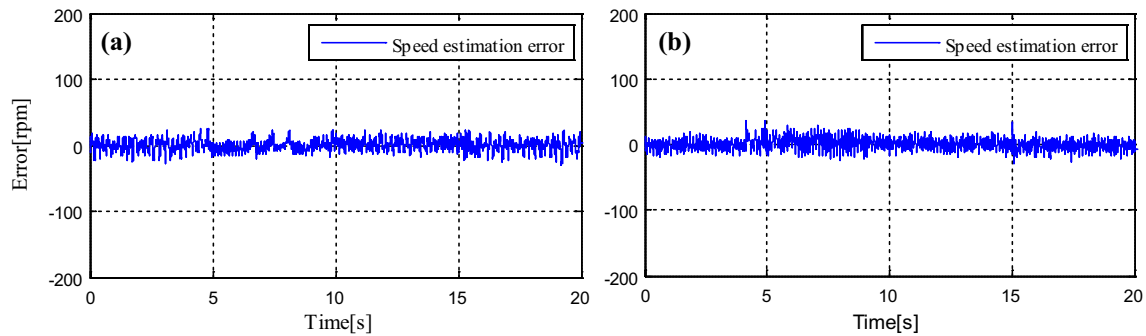
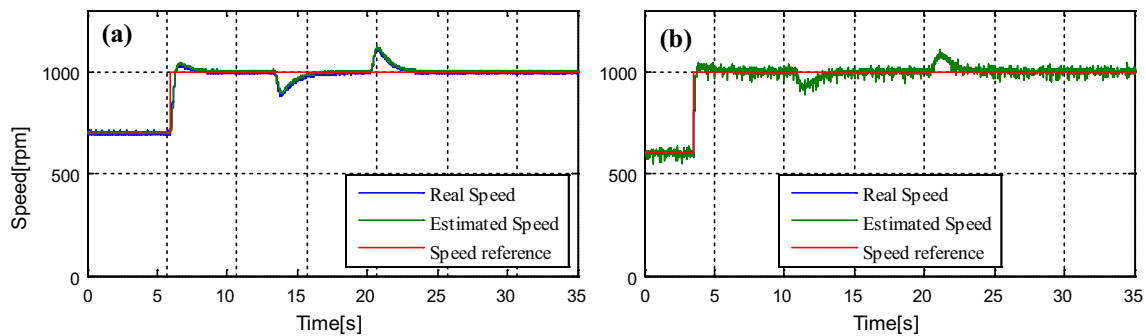**Fig. 16** Speed estimation errors: **a** FL based ALO, **b** PI based ALO



**Fig. 17** Effect of step load torque variation on speed responses using: **a** FL based ALO, **b** PI based ALO
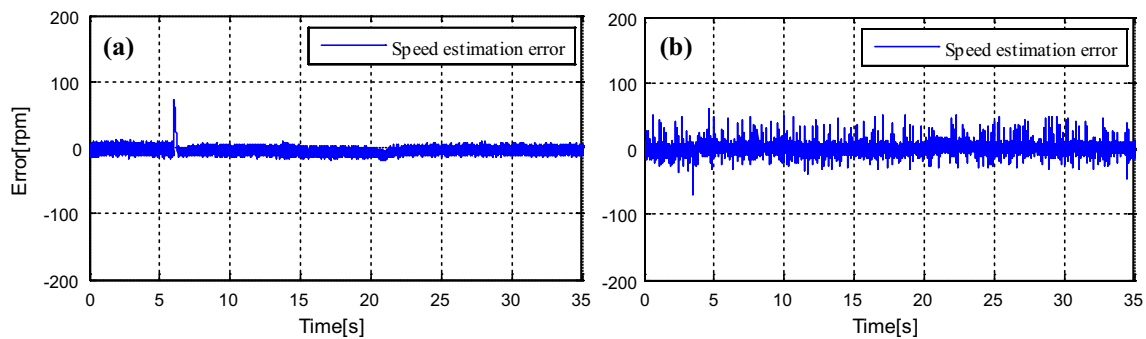


**Fig. 18** Speed estimation errors: **a** FL based ALO, **b** PI based ALO

### 4.7 Parameters Identification in the Presence of Load Torque Variation

The motor speed is running at 300 rpm as shown in Fig. 27 and a load torque of 0,5 N.m is introduced at 12 s to achieve 1 N.m. The test objective is to show performances of the proposed sensorless drive with online parameters estimation in the presence of load torque and stator resistance variations. The stator resistance value is increased at 4 s by 5.5 Ω to reach 12 Ω and decreased by 5.5 Ω after some few seconds.

Figures 28, 29 and 30 show very satisfying performances using FL based ALO. Furthermore, the experimental results show that the estimated speed and stator resistance obtained with FL based ALO are slightly affected by the load torque variation compared to the ones obtained with the PI based ALO.
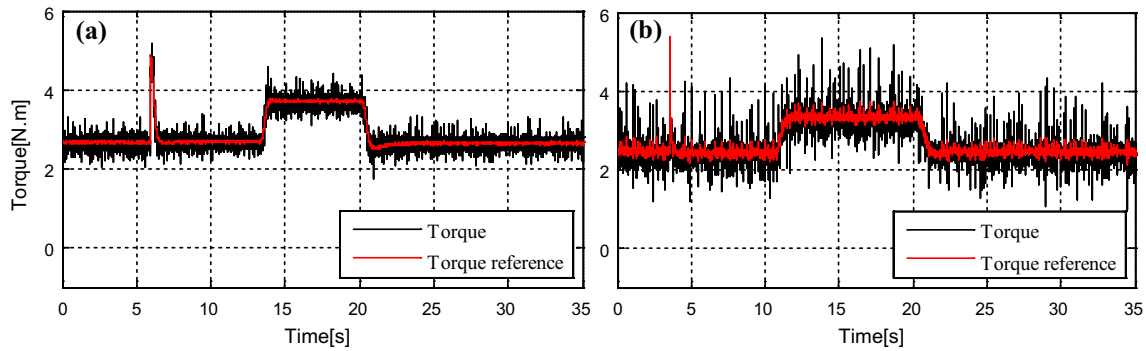
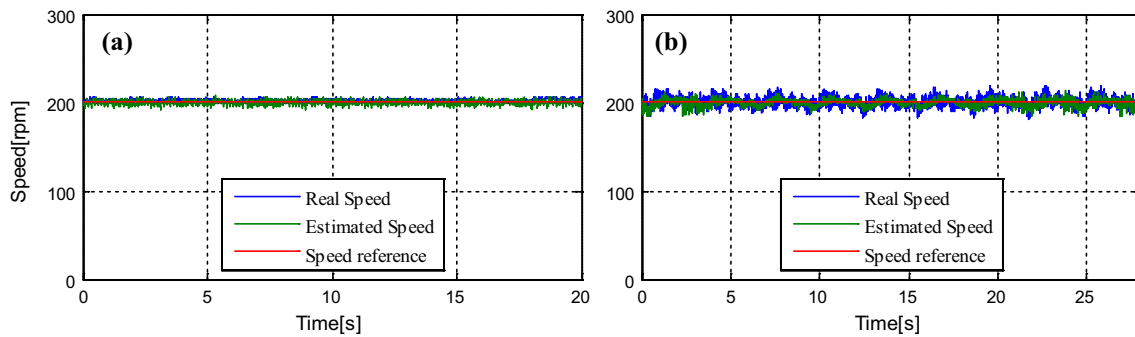**Fig. 19** Electromagnetic torque responses using: **a** FL based ALO, **b** PI based ALO



**Fig. 20** Speed responses in the presence of stator resistance and RTC inverse estimation (off load) using: **a** FL based ALO, **b** PI based ALO
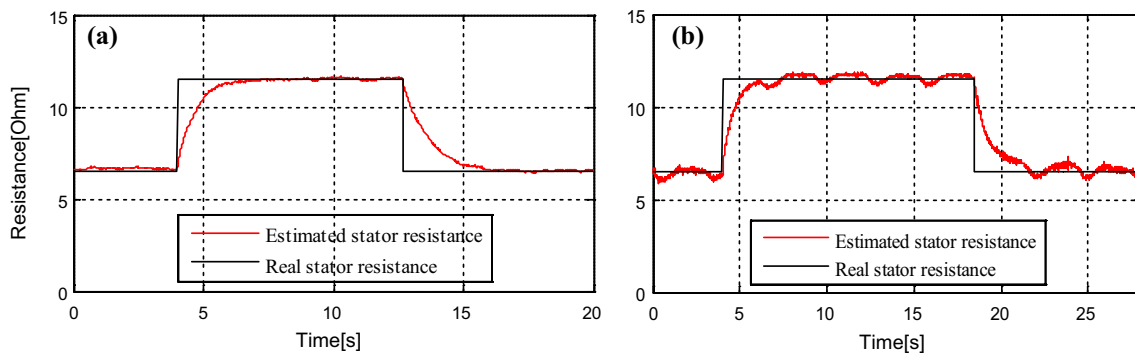


**Fig. 21** Responses of the estimated stator resistance (off load) using: **a** FL based ALO, **b** PI based ALO

With regard to the electromagnetic torque, a comparison between the two developed electromagnetic torques in Fig. 29 shows a strong reduction of the torque ripples using the FL based ALO with respect to the PI based ALO.

Finally, the experimental results has shown high improvements achieved by this proposed observer. The consequent main advantage is obviously the reduction of ripples in the estimated speed and/or the electromagnetic torque and the preservation of all the advantages of the PI based ALO namely stability in all speed ranges and dynamic performances.
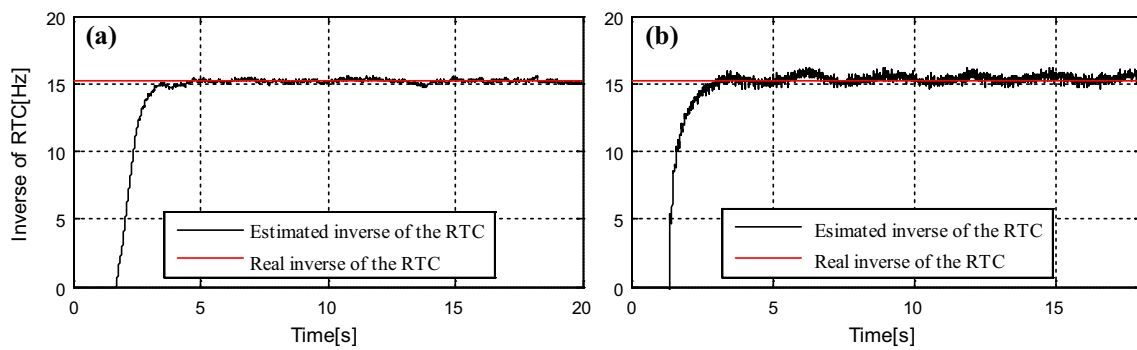
**Fig. 22** Responses of the estimated inverses of the RTC (off load) using: **a** FL based ALO, **b** PI based ALO
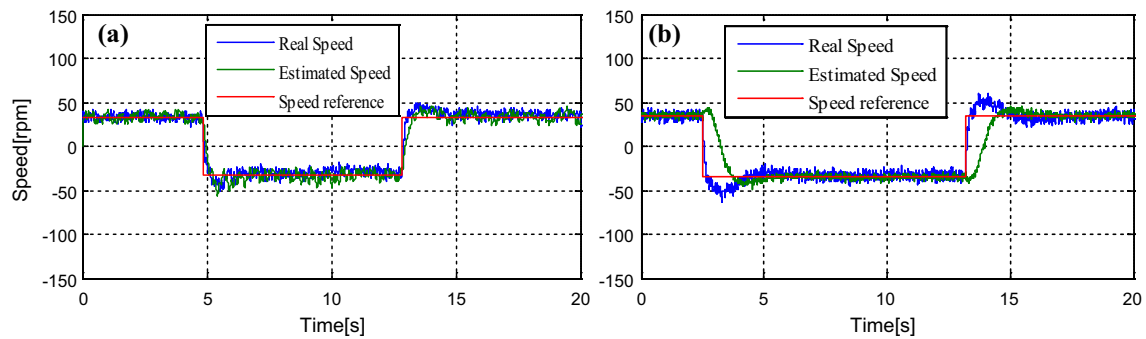


**Fig. 23** Speed responses at very low speeds (off load) using: **a** FL based ALO, **b** PI based ALO
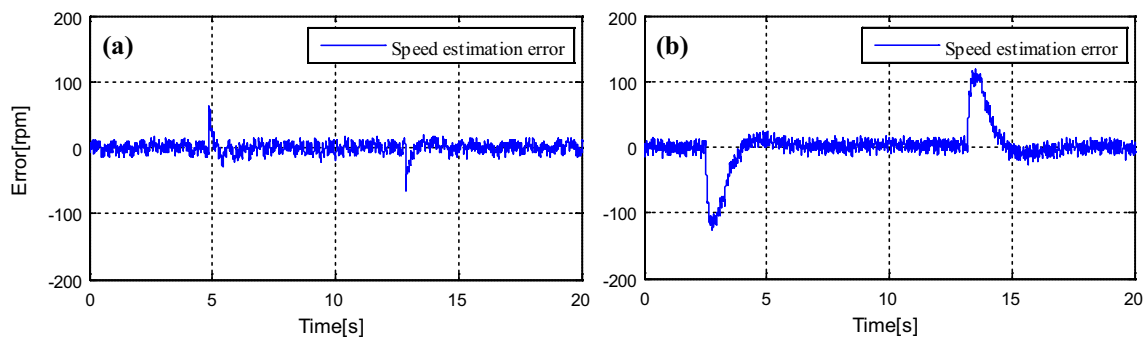


**Fig. 24** Speed estimation errors: **a** FL based ALO, **b** PI based ALO

# 5 Conclusion

This paper proposes an improved speed estimation method for sensorless induction motor drive using an improved adaptive Luenberger observer with parameters identification using fuzzy logic techniques.

The stability of the proposed sensorless indirect field oriented control with stator resistance and rotor time
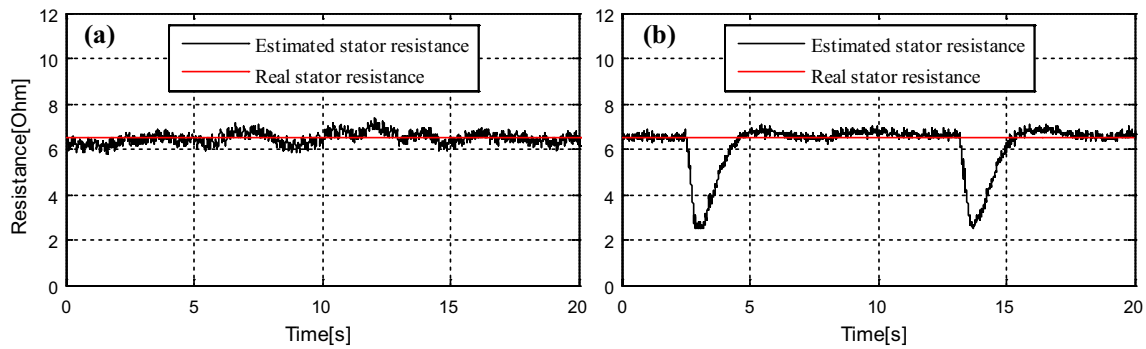
**Fig. 25** Responses of the estimated stator resistance at very low speeds (off load) using: **a** FL based ALO, **b** PI based ALO
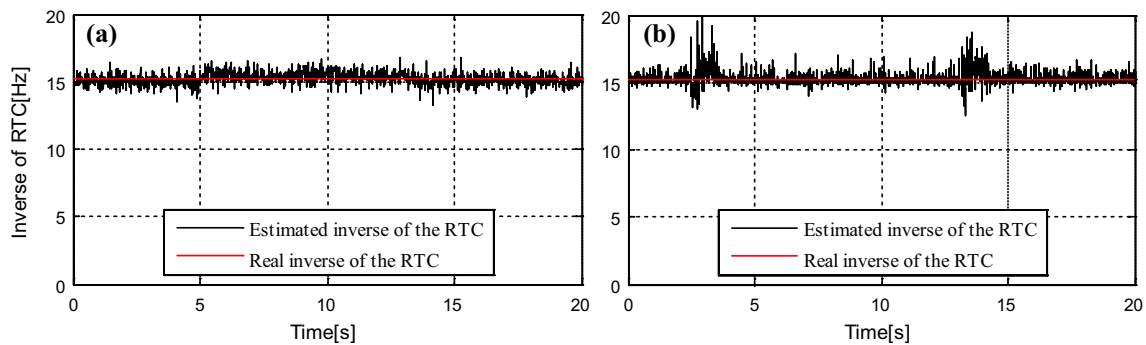


**Fig. 26** Responses of the estimated inverses of the RTC at very low speeds (off load) using: **a** FL based ALO, **b** PI based ALO
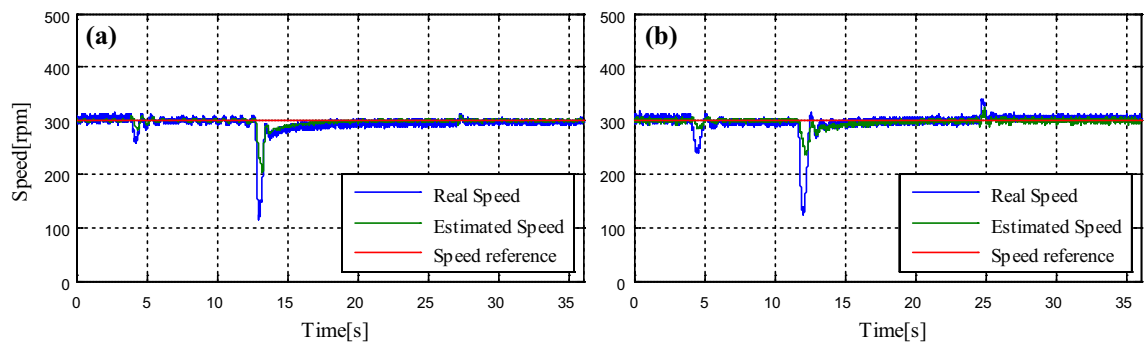


**Fig. 27** Speed responses in the presence of stator resistance and load torque variations using: **a** FL based ALO, **b** PI based ALO

constant tuning has been demonstrated by Lyapunov criterion and its validity has been proved by experimentation applied to an 1 kW squirrel-cage induction motor for a wide range of speed under load and no load.

The experimental results highlight clearly the effectiveness of the proposed system in terms of dynamic performance at high and very low speed regions during transient and steady states and its robustness against IM parameters uncertainties.
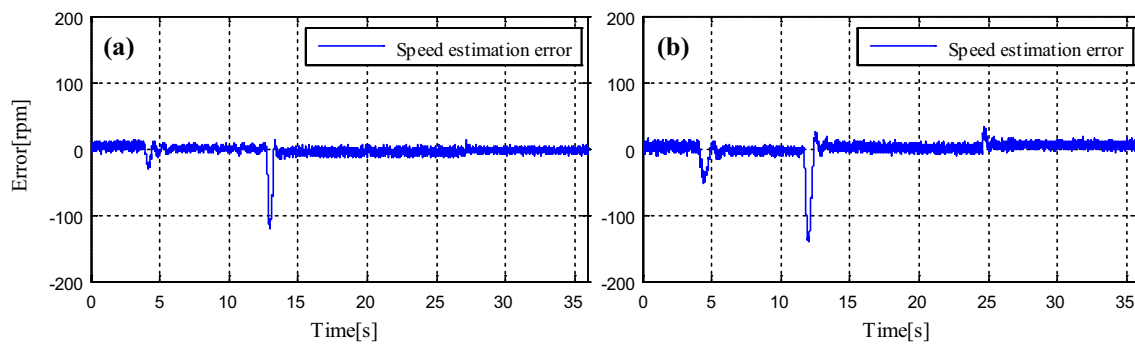
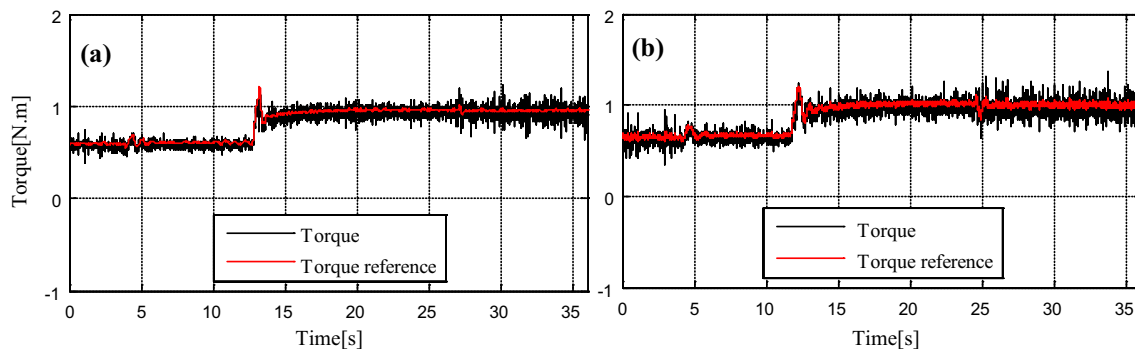Fig. 28 Speed estimation errors: **a** FL based ALO, **b** PI based ALO

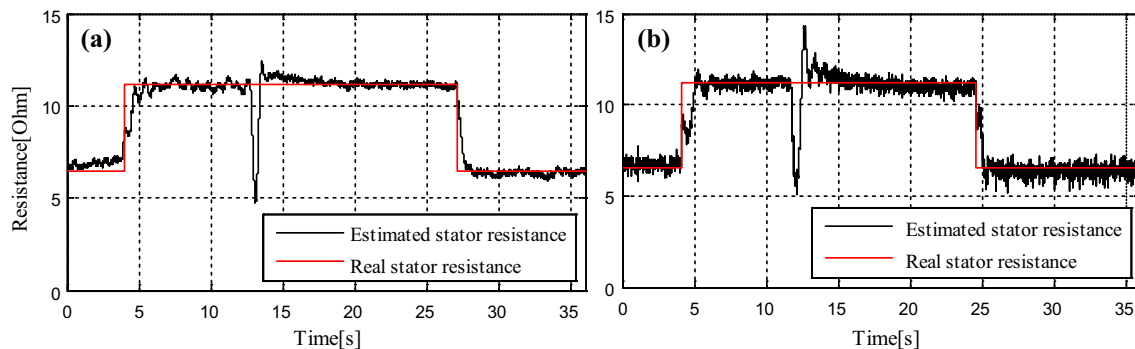Fig. 29 Electromagnetic torque responses using: **a** FL based ALO, **b** PI based ALO

Fig. 30 Responses of the estimated stator resistance in the presence of load torque variations using: **a** FL based ALO, **b** PI based ALO

Further research work includes the implementation of the proposed technique in another powerful and less expensive DSP processor for industrial applications.

## References

1. Abdelwanis MI, El-Sehiemy RA (2019) A fuzzy-based controller of a modified six-phase induction motor driving a pumping system. Iran J Sci Technol Trans Electr Eng 43:153–165

2. Agrebi Zorgani Y, Koubaa Y, Boussak M (2016) MRAS state estimator for speed sensorless ISFOC induction motor drives with Luenberger load torque estimation. ISA Trans 61:308–317

3. Alonge F, Cangemi T, D'Ippolito F, Fagiolini A, Sferlazza A (2015) Convergence analysis of extended kalman filter for sensorless control of induction motor. IEEE Trans Ind Electron 62:2341–2352

4. Ameid T, Menacer A, Talhaoui H, Harzellia I (2017) Rotor resistance estimation using Extended Kalman filter and spectral analysis for rotor bar fault diagnosis of sensorless vector control induction motor. Measurement 111:243–259

5. Banarezaei S, Shalchian M (2019) Design of a model-based fuzzy-pid controller with self-tuning scalingfactor for idle speed control of automotive engine. Iran J Sci Technol Trans Electr Eng 43:13–31

6. Cirrincione M, Pucci M, Vitale G (2012) Power converters and AC electrical drives with linear neural networks. CRC Press, Florida, pp 531–603

7. Cirrincione M, Accetta A, Pucci M, Vitale G (2013) MRAS speed observer for high-performance linear induction motor drives based on linear neural networks. IEEE Trans Power Electr 28:123–134

8. Derdiyok A, Güven MK, Rehman H, Inanc N, Xu L (2002) Design and implementation of a new sliding-mode observer for speed-sensorless control of induction machine. IEEE Trans Ind Electron 49:1177–1182

9. Gacho J, Žalman M (2010) IM based speed servodrive with luenberger observer. J Electr Eng 61:149–156

10. Gadoue SM, Giaouris D, Finch J (2010) MRAS sensorless vector control of an induction motor using new sliding-mode and fuzzy-logic adaptation mechanisms. IEEE Trans Energy Conver 25:394–402

11. Habibullah M, Lu DDC (2015) A speed-sensorless FS-PTC of Induction motors using extended kalman filters. IEEE Trans Ind Electron 62:6765–6778

12. Hadj Saïd S, Mimouni M, M'Sahli F, Farza M (2011) High gain observer based on-line rotor and stator resistances estimation for IMs. Simul Model Pract Th 19:1518–1529

13. Hazzab A, Bousserhane IK, Zerbo M, Sicard P (2006) Real time implementation of fuzzy gain scheduling of pi controller for induction motor machine control. Neural Process Lett 24:203–215

14. Hinkkanen M, Leppanen VM, Luomi J (2005) Flux observer enhanced with low-frequency signal injection allowing sensorless zero-frequency operation of induction motors. IEEE Trans Ind Appl 41:52–59

15. Inanc N (2007) A robust sliding mode flux and speed observer for speed sensorless control of an indirect field oriented induction motor drives. Electr Pow Syst Res 77:1681–1688

16. Jouili M, Agrebi Y, Koubaa Y, Boussak M (2015) A Luenberger state observer for simultaneous estimation of speed and stator resistance in sensorless IRFOC induction motor drives. In: IEEE 16th international conference on sciences and techniques of automatic control and computer engineering (STA), pp 898–904. https://doi.org/10.1109/STA.2015.7505225

17. Jouili M, Jarray K, Koubaa Y, Boussak M (2012) Luenberger state observer for speed sensorless ISFOC induction motor drives. Electr Pow Syst Res 89:139–147

18. Kubota H, Matsuse K, Nakmo T (1993) DSP-based speed adaptive flux observer of induction motor. IEEE Trans Ind Appl 29:344–348

19. Kubota H, Matsuse K (1994) Speed sensorless field-oriented control of induction motor with rotor resistance adaptation. IEEE Trans Ind Appl 30:1219–1224

20. Lokriti A, Salhi I, Doubabi S, Zidani Y (2013) Induction motor speed drive improvement using fuzzy IP-self-tuning controller. A real time implementation. ISA Trans 52:406–417

21. Luenberger DG (1971) An introduction to observers. IEEE Trans Automat Contr 16:596–602

22. Maes J, Melkebeek JA (2000) Speed-sensorless direct torque control of induction motors using an adaptive flux observer. IEEE Trans Ind Appl 36:778–785

23. Maiti S, Verma V, Chakraborty C, Hori Y (2012) An adaptive speed sensorless induction motor drive with artificial neural network for stability enhancement. IEEE Trans Ind Inform 8:757–766

24. Pacas Mario (2011) Sensorless drives in industrial applications". IEEE Ind. Electron. Mag. 5(2):16–23

25. Zaky MS, Metwally MK, Azazi HZ, Deraz SA (2018) A new adaptive SMO for speed estimation of sensorless induction motor drives at zero and very low frequencies. IEEE Trans Ind Electron 65(9):6901–6911

26. Mohand Ouhrouche, Rachid Errouissi, Andrzej M. Trzynadlowski, Kambiz Arab Tehrani, Ammar Benzaioua (2016) A Novel Predictive Direct Torque Controller for Induction Motor Drives" IEEE Transactions on Industrial Electronics, 2016, Vol : 63, Issue: 8

27. Moutchou M, Abbou A, Mahmoudi H (2015) MRAS-based sensorless speed backstepping control for induction machine, using a flux sliding mode observer. Turk J Electr Eng Co 23:187–200

28. Mihai C (2016) Design and implementation of a highly robust sensorless sliding mode observer for the flux magnitude of the induction motor. IEEE Trans Energy Conv 31(2):649–657

29. Naik NV, Panda A, Singh SP (2016) A three-level fuzzy-2 DTC of induction motor drive using SVPWM. IEEE Trans Ind Electron 63(3):1467–1479

30. Qu Z, Hinkkanen M, Harnefors L (2014) Gain scheduling of a full-order observer for sensorless induction motor drives. IEEE Trans Ind Appl 50:3834–3845

31. Rafa S, Larabi A, Barazane L, Manceur M, Essounbouli N, Hamzaoui A (2014) Implementation of a new fuzzy vector control of induction motor. ISA Trans 53:744–754

32. Ramesh T, Panda AK, Shiva Kumar S (2015) Type-2 fuzzy logic control based MRAS speed estimator for speed sensorless direct torque and flux control of an induction motor drive. ISA Trans 57:262–275

33. Rayyam M, Zazi M, Barradi Y (2018) A new metaheuristic unscented Kalman filter for state vector estimation of the induction motor based on Ant Lion optimizer. COMPEL Int J Comput Math Electr Electron Eng 37:1054–1068

34. Samadi M, Rakhtala SM (2019) Reducing cost and size in photovoltaic systems using three-level boost converter based on fuzzy logic controller. Iran J Sci Technol Trans Electr Eng 43:313–323. https://doi.org/10.1007/s40998-018-0145-6

35. Smith AN, Gadoue SM, Finch JW (2016) Improved rotor flux estimation at low speeds for torque mras-based sensorless induction motor drives. IEEE Trans Energy Conver 31:270–282

36. Vasić V, Vukosavic S, Levi E (2003) A stator resistance estimation scheme for speed sensorless rotor flux oriented induction motor drives. IEEE Trans Energy Conver 18:476–483

37. Zadeh LA (1965) Fuzzy sets. Inf Control 28:338–353

38. Zbede YB, Gadoue SM, Atkinson DJ (2016) Model Predictive MRAS Estimator for Sensorless Induction Motor Drives. IEEE Trans Ind Electron 63:3511–3521

**Zakaria Boulghasoul** was born in Essaouira, Morocco in 1986. He received the M.S. degree in electrical engineering in 2009 from Cadi Ayyad University, Morocco and the Ph.D. degree in electrical engineering in 2014 from Ph.D. Center of engineering sciences in the same university. Currently he is an Assistant professor of Power Electronics and Electrical Drive at the National School of Applied Sciences of Marrakech, Cadi Ayyad University. His area of interest is related to the innovative control strategies for AC Drives, especially Induction Motor Drives, Predictive Control, Neural Network, Fuzzy logic and Sensorless Control.

**Zineb Kandoussi** was born in Settat in Morocco, on April 24, 1988. In 2011, she got her engineer degree in Electrical Engineering from the National School of Applied Sciences of Marrakech, Cadi Ayyad University, Morocco. In October 2013, she embarked on the Ph.D. research in the Ph.D. Center of engineering sciences in the same university. She got her Ph.D. degree in Induction Motor Control in 2018. Her employment experience included the Safran Aerosystems international company, she worked there as a software development engineer for two years and a half. Currently, she is a professor at the Private University of Marrakech. Her special fields of interest included sensorless control strategies of AC Drives and embedded software.

**Abdelhadi Elbacha** was born in Zagora, Morocco, in 1975. He received the B.S. degree and the Aggregation in electrical engineering from ENSET Rabat, Morocco in 1995 and 1999 respectively, and then he received the M.S. degree in industrial informatics and the Ph.D. degree in electrical engineering from Cadi Ayyad University, Morocco, in 2001 and 2006 respectively. Currently, he is an HDR Professor of Power Electronics and Motor control at the National School of Applied Sciences of Marrakech, Cadi Ayyad University. His current area of interest is related to the innovative control strategies for AC Drives, especially Induction Motor Drives and Sensorless Control.

**Abdelouahed Tajer** was born in Morocco in 1977. After a Master degree in Systems Optimization and Safety at the University of Reims Champagne Ardenne / University of technology of Troyes in France, he achieved a Ph.D. degree in Control of Discrete-events Systems at the University of Reims Champagne-Ardenne in France in 2005. His research interests are: Discrete Event Systems, Fault diagnosis, Modeling, Supervisory Control Theory, Optimal Control, Manufacturing systems. Currently, he is a full professor at the National School of Applied Sciences of Marrakech, Cadi Ayyad University, Morocco.